Archive of Applied Mechanics (2024) 94:221–237
https://doi.org/10.1007/s00419-023-02517-x

ORIGINAL

**Luji Wu · Wei Feng · Linjie Yang · Huaiwen Yang · Shihao Yang · Baoguo Liu**

# Dynamic modeling and vibration analysis of herringbone gear system with uncertain parameters

Received: 30 November 2022 / Accepted: 17 November 2023 / Published online: 13 December 2023
© The Author(s), under exclusive licence to Springer-Verlag GmbH Germany, part of Springer Nature 2023

**Abstract** There are inevitably all kinds of uncertainties in the gear transmission system. These uncertainties will have an important impact on the vibration response of the system. In this paper, the vibration response characteristics of herringbone gear transmission system with uncertain parameters are investigated. A six-degree-of-freedom dynamic model of single-stage herringbone gear-shaft-bearing system is established based on the finite element method. The stochastic agent model of the system is constructed by polynomial chaotic expansion (PCE), and the effects of gear meshing stiffness, bearing stiffness and damping parameters uncertainty on the vibration response of the system are analyzed. The results show that the uncertainty of gear meshing stiffness leads to the offset of the boundary value of the vibration amplitude of the system, and the uncertainty of bearing damping mainly affects the vibration amplitude of the main resonance region of the system. The uncertainty of bearing stiffness has little effect on the vibration amplitude of the system. And the hybrid uncertainty has comprehensive effect on the vibration amplitude of the system.

**Keywords** Herringbone gear · Dynamic modeling · Vibration analysis · Uncertain parameters

## 1 Introduction

Herringbone gear is widely used in aviation, heavy machinery transmission and other fields, due to its small meshing impact, smooth transmission torque, high bearing capacity, and low axial force [1]. The dynamic characteristics of gear transmission directly affect the working performance of the whole equipment. With the development of mechanical equipment to large-scale, high reliability, high precision and long life, the requirements for the dynamic performance of gear transmission system are also increasing. It is becoming more and more important to accurately predict the dynamic performance of the system. In-depth dynamic research on the gear transmission system can lay a foundation for the safety, optimal design, and reliability evaluation of the mechanical equipment.

Extensive research works have been done on dynamic modeling and vibration analysis of gear transmission system [2, 3]. For the dynamics of herringbone gear transmission system, Choi et al. [4] used the finite element method to analyze the transverse, torsional and axial vibration characteristics of herringbone teeth. Sondkar and Kahraman [5] put forward a three-dimensional dynamic model of herringbone gear planetary system with gear meshing, bearing, and supporting accessories, and studied the effects of planetary phase angle, error

L. Wu · W. Feng (✉) · L. Yang · S. Yang
Zheng Zhou Research Institute of Mechanical Engineering CO., LTD, Zhengzhou 450001, China
e-mail: wfeng@haut.edu.cn

L. Wu
School of Mechanical Engineering, Tongji University, Shanghai 200092, China

W. Feng · H. Yang · B. Liu
School of Electromechanical Engineering, Henan University of Technology, Zhengzhou 450001, China

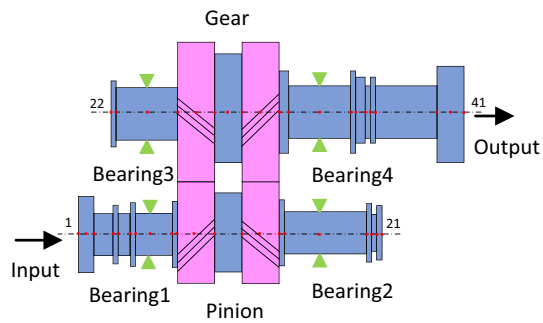


**Fig. 1** Schematic diagram of the herringbone system

and gear supporting conditions on the dynamic response of gear system. Chen et al. [6, 7] investigated the influence of runout and pitch error on the dynamic response of herringbone gear. Wang et al. [8] established a dynamic model of double helical gears considering axial vibration and side clearance. Dong et al. [9] built up a dynamic model of herringbone teeth based on Timoshenko beam and lumped parameter method, and verified it by experiments. Wang et al. [10] presented a model of double helical gears by taking the axial vibration and backlash into account. Liu et al. [11] developed an improved dynamic analysis model of double helical gear reducer using hybrid user-defined element method (HUELM). Yin et al. [12, 13] developed a bending–torsional–axial coupling model for dynamic analysis of double-helical gear system. They then carried out theoretical and experimental research on the dynamic characteristics of herringbone gear system by considering the oil film effect among meshing teeth.

However, most of the above researches on gear system dynamics are treated as deterministic problems. In practical engineering, uncertain factors widely exist in mechanical systems such as gear transmission [14–17], due to errors in manufacturing, processing, assembly, wear, lubrication and changes in operating environment. These uncertainties will affect the dynamic characteristics of the gear system. Guerine et al. [18] investigated the effects of random uncertainty of mass, damping coefficient, bending stiffness and torsion stiffness on the dynamic response of single-stage spur gear system. Yang et al. [19] studied the dynamic characteristics of gear transmission system under the combined action of deterministic and random excitations. Beyaoui et al. [20] explored the impact of random perturbation caused by aerodynamic torque excitation on the dynamic response of fan gear system. Mabrouk et al. [21] investigated the dynamic behavior of a bevel gear system with uncertainty associated to the performance coefficient of the input aerodynamic torque based on the projection on polynomial chaos. Fang et al. [22] proposed a dynamic model of spur gear pair and investigated the random effects of load and friction on its transient characteristics. Hajnayeb and Sun [23] studied the vibration caused by random machining error of gear tooth profile based on a simplified model of gear pair, and obtained the transfer function between manufacturing error and common measuring position. Wei et al. [24] provided a dynamic model of spur gear system with uncertain parameters, and studied the dynamic response of the system by using Chebyshev inclusion function. Fu et al. [25] explored the dynamic characteristics of wind turbines system under aleatory and epistemic uncertainties.

The above researches on the dynamic uncertainty of gear system are mainly focused on the spur gear system, while the research on the uncertainty of herringbone gear system is relatively less. In addition, most of the above studies are based on the pure torsion dynamic model of gear. In this paper, a dynamic model of herringbone gear-shaft-bearing system is established. The uncertainty of the system is modeled by PCE method, and the effects of gear meshing stiffness, bearing stiffness, and damping on the vibration response of the system are analyzed.

## 2 Dynamic model of gear transmission system

The herringbone gear transmission system investigated in this paper is shown in Fig. 1, which consists of a pair of herringbone gears, two gear shafts and two pairs of journal bearings. The design parameters of the system are listed in Table 1.

**Table 1** Design parameters of the herringbone system

| Parameter | Pinion | Gear |
|---|---|---|
| Gear | | |
| Teeth number | 46 | 93 |
| Module (mm) | 7 | |
| Pressure angle (°) | 25 | |
| Helix angle (°) | 23.38 | |
| Face width (mm) | 205 | 200 |
| Shaft | | |
| Diameter of axis segment from left to right (mm) | 410, 200, 240, 200, 240, 200, 300, 364, 300, 364, 300, 200, 240, 120, 195 | 290, 250, 723, 630, 723, 360, 250, 360, 290, 250, 290, 250, 548 |
| Length of axis segment from left to right (mm) | 105, 113, 24, 31, 25, 237, 15, 205, 100, 205, 15, 290, 30, 23, 17 | 24, 313, 200, 100, 200, 40, 200, 15, 41, 17, 24, 250, 548 |
| Material parameter | | |
| Young's modulus (GPa) | 210 | |
| Poisson's ratio | 0.3 | |

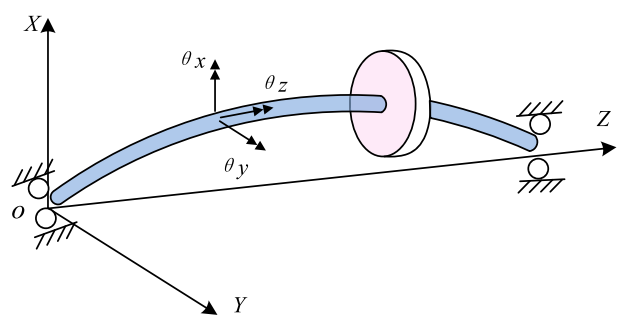


**Fig. 2** Typical rotor configuration and coordinate system

## 2.1 Shaft model

As shown in Fig. 2, the shaft model is based on Timoshenko beam element by using the finite element method, which is divided into 41 nodes, each node has 6 degrees of freedom, including three translations and two rotations, expressed as $x$, $y$, $z$, $\theta$x, $\theta$y and $\theta$z. Using the Lagrange equation, the free vibration equation of the rotor can be expressed as

$$\boldsymbol{M}_s\ddot{\boldsymbol{X}}_s + \boldsymbol{C}_s\dot{\boldsymbol{X}}_s + \boldsymbol{K}_s\boldsymbol{X}_s = 0, \tag{1}$$

where $\boldsymbol{M}$s, $\boldsymbol{C}$s and $\boldsymbol{K}$s are the mass matrix, damping matrix and stiffness matrix of shaft, respectively.

The mass matrix of the shaft $\boldsymbol{M}$s can be written as:

$$\boldsymbol{M}_{\mathrm{s}} = \mathrm{diag}\left\{m_{s1},\ m_{s1},\ m_{s1},\ I_{xs1},\ I_{ys1},\ I_{zs1},\ m_{s2},\ m_{s2},\ m_{s2},\ I_{xs2},\ I_{ys2},\ I_{zs2}\right\},$$

where $m_{\mathrm{si}}$ and $I_{\mathrm{ski}}$ are the mass and moment of inertia of the $i$th beam element, respectively, $i = 1,2$, $k = x$, $y$, $z$.

According to the theory of elasticity, the $12 \times 12$ stiffness matrix of Timoshenko beam element $\boldsymbol{K}$s can be obtained.

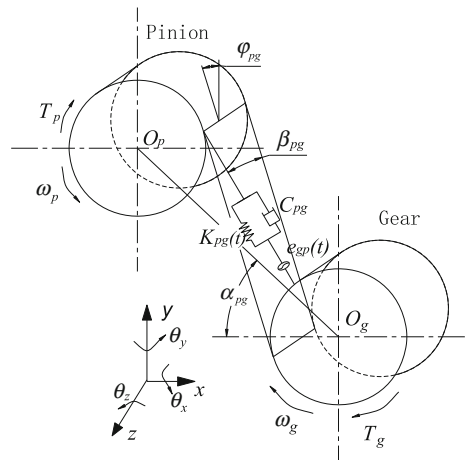


**Fig. 3** Gear mesh model

$$\boldsymbol{K}_s = \begin{bmatrix} \frac{AE}{L} & & & & & & & & & & \\ 0 & a_x & & & & & & & & & \\ 0 & 0 & a_y & & & & & & & & \\ 0 & 0 & 0 & \frac{GJ}{L} & & & & & \text{Sym} & & \\ 0 & 0 & -c_y & 0 & e_y & & & & & & \\ 0 & c_x & 0 & 0 & 0 & e_x & & & & & \\ -\frac{AE}{L} & 0 & 0 & 0 & 0 & 0 & \frac{AE}{L} & & & & \\ 0 & -a_x & 0 & 0 & 0 & -c_x & 0 & a_x & & & \\ 0 & 0 & -a_y & 0 & c_y & 0 & 0 & 0 & a_y & & \\ 0 & 0 & 0 & \frac{GJ}{L} & 0 & 0 & 0 & 0 & 0 & \frac{GJ}{L} & \\ 0 & 0 & -c_y & 0 & f_y & 0 & 0 & 0 & c_y & 0 & e_y \\ 0 & c_x & 0 & 0 & 0 & f_x & 0 & -c_x & 0 & 0 & 0 \; e_x \end{bmatrix}. \tag{2}$$

$$\begin{cases} a_x = a_y = \frac{12EI}{L^3(1+\varphi)}, c_x = c_y = \frac{6EI}{L^2(1+\varphi)} \\ e_x = e_y = \frac{(4+\varphi)EI}{L(1+\varphi)}, f_x = f_y = \frac{(2-\varphi)EI}{L(1+\varphi)} \end{cases} \tag{3}$$

where $E$ is the Young's modulus; $\mu$ is the Poisson's ratio; $A$ is the element cross-sectional area; $L$ is the element length; $G$ is the shear modulus; $J$ is the torsional moment of inertia; $I$ is the moment of inertia of diameter; $\varphi$ is the shear influence factor, $\varphi = 12EI/(GAKL^2)$; $K$ is the shearing coefficient, $K = 6(1 + \mu)/ (7 + 6\mu)$.

The damping matrix of the shaft can be expressed as $\boldsymbol{C}\text{s} = \boldsymbol{\gamma K}\text{s}$, where $\gamma$ is the proportional damping coefficient, where $\gamma$ is $1 \times 10^{-5}$ [26].

## 2.2 Gear model

### *2.2.1 Gear model*

The gear mesh model is shown in Fig. 3, the gear consists of a pinion and a gear, which are represented by mesh stiffness $k_{\text{pg}}$ and meshing damping $c_{\text{pg}}$ along the mesh line. The rotation angular velocity of the pinion and gear are $\omega_1$ and $\omega_2$, respectively. The torque of the pinion and gear are $T_1$ and $T_2$, respectively. The static transmission error of gear $e_{\text{pg}}$(t) can be expressed as

$$e_{\text{pg}}(t) = e_{\text{pg}} \sin(\omega_{\text{p}} z_{\text{p}} t), \tag{4}$$

The relative displacement of the gear pair along the line of action can be written as

$$\begin{aligned}\boldsymbol{V} = [&\cos\beta_{\mathrm{pg}}\sin\varphi_{\mathrm{pg}},\ \pm\cos\beta_{\mathrm{pg}}\cos\varphi_{\mathrm{pg}},\ \sin\beta_{\mathrm{pg}},\ \mp r_{\mathrm{p}}\sin\beta_{\mathrm{pg}}\sin\varphi_{\mathrm{pg}},\\ &r_{\mathrm{bp}}\sin\beta_{\mathrm{pg}}\cos\varphi_{\mathrm{pg}},\ \pm r_{\mathrm{bp}}\cos\beta_{\mathrm{pg}},\ -\cos\beta_{\mathrm{pg}}\sin\varphi_{\mathrm{pg}},\ \mp\cos\beta_{\mathrm{pg}}\cos\varphi_{\mathrm{pg}},\\ &-\sin\beta_{\mathrm{pg}},\ \mp r_{\mathrm{bg}}\sin\beta_{\mathrm{pg}}\sin\varphi_{\mathrm{pg}},\ -r_{\mathrm{bg}}\sin\beta_{\mathrm{pg}}\cos\varphi_{\mathrm{pg}},\ \pm r_{\mathrm{bg}}\cos\beta_{\mathrm{pg}}]\end{aligned} \tag{5}$$

where $r_{bp}$ and $r_{bg}$ are the radius of the base circle of the pinon and the gear; $\beta$ is the helix angle of the base circle; $\varphi_{pg}$ is the angle between the end joint line and the y-axis, which varies with the rotation of the pinon

$$\varphi_{\mathrm{pg}} = \begin{cases}\varphi_{\mathrm{pg}} - \alpha_{\mathrm{pg}} & \text{counterclockwise}\\ -\varphi_{\mathrm{pg}} + \alpha_{\mathrm{pg}}, & \text{clockwise}\end{cases}, \tag{6}$$

The motion coupling equation of gear pair can be expressed as

$$\boldsymbol{M}_{\mathrm{pg}}\ddot{\boldsymbol{X}}_{\mathrm{pg}} + \left(\boldsymbol{C}_{\mathrm{pg}} + \boldsymbol{G}_{\mathrm{pg}}\right)\dot{\boldsymbol{X}}_{\mathrm{pg}} + \boldsymbol{K}_{\mathrm{pg}}\boldsymbol{X}_{\mathrm{pg}} = \boldsymbol{F}_{\mathrm{m}}, \tag{7}$$

where $\boldsymbol{M}_{\mathrm{pg}}$ is the gear mass matrix; $\boldsymbol{C}_{\mathrm{pg}}$ is the gear mesh damping matrix; $\boldsymbol{G}_{\mathrm{pg}}$ is the gyroscopic matrix; $\boldsymbol{K}_{\mathrm{pg}}$ is the mesh stiffness matrix; $\boldsymbol{F}_{\mathrm{m}}$ is the static transmission error excitation. They can be written as

$$\boldsymbol{M}_{\mathrm{pg}} = \mathrm{diag}\left\{m_p, m_p, m_p, I_{xp}, I_{yp}, I_{zp}, m_g, m_g, m_g, I_{xg}, I_{yg}, I_{zg}\right\}, \tag{8}$$

$$\boldsymbol{X}_{\mathrm{pg}} = \left\{x_{\mathrm{p}}, y_{\mathrm{p}}, z_p, \theta_{xp}, \theta_{yp}, \theta_{zp}, x_g, y_g, z_g, \theta_{xg}, \theta_{yg}, \theta_{zg}\right\}^{\mathrm{T}}, \tag{9}$$

$$\boldsymbol{K}_{\mathrm{pg}} = k_{\mathrm{pg}}.\boldsymbol{V}^T.\boldsymbol{V}, \tag{10}$$

$$\boldsymbol{C}_{\mathrm{pg}} = C_{\mathrm{pg}}.\boldsymbol{V}^T.\boldsymbol{V}, \tag{11}$$

$$\boldsymbol{G}_{\mathrm{pg}} = \begin{bmatrix}\boldsymbol{g}_{\mathrm{p}} & 0\\ 0 & \boldsymbol{g}_{\mathrm{g}}\end{bmatrix}, \tag{12}$$

$$\boldsymbol{g}_{p,g} = \begin{bmatrix}0 & 0 & 0 & 0 & 0 & 0\\ 0 & 0 & 0 & 0 & 0 & 0\\ 0 & 0 & 0 & 0 & 0 & 0\\ 0 & 0 & 0 & I_{zp,g}\omega_{p,g} & 0 & 0\\ 0 & 0 & -I_{zp,g}\omega_{p,g} & 0 & 0 & 0\\ 0 & 0 & 0 & 0 & 0 & 0\end{bmatrix}, \tag{13}$$

$$\boldsymbol{F}_{\mathrm{m}} = k_{\mathrm{pg}}\boldsymbol{V}^T e_{\mathrm{pg}}(t) + c_{\mathrm{pg}}\boldsymbol{V}^T\dot{e}_{\mathrm{pg}}(t), \tag{14}$$

$$\boldsymbol{F} = \left[0\ 0\ 0\ 0\ 0\ T_{\mathrm{p}}\ 0\ 0\ 0\ 0\ 0\ T_{\mathrm{g}}\right], \tag{15}$$

### *2.2.2 Gear mesh stiffness*

The main calculation methods for gear mesh stiffness include the potential energy method, the finite element method and the Ishikawa method [27]. Although the calculation cost of the finite element method is high, its calculation result is relatively more accurate. In this subsection, the gear mesh stiffness is obtained by using the finite element method. In order to reduce the calculation time, only the three-dimensional local mesh model of the gear is established, as shown in Fig. 4. Ignoring the influence of tooth profile error on contact analysis, the static transmission error during load is equal to the deformation of gear teeth, and the mesh stiffness $K_n$ of gear can be expressed as the ratio of the load on the gear to the mesh deformation of gear teeth

$$K_n = \frac{F_n}{\delta_n}, \tag{16}$$

where $F_n$ is the normal load of the tooth surface; $\delta_n$ is the normal comprehensive elastic deformation of the tooth surface, which includes the contact elastic deformation caused by the local Hertz contact, the contact position deformation caused by the loaded bending of the gear teeth and the contact position displacement caused by the hub deformation [28].

Consider a mesh cycle where the pinon from the mesh of one gear tooth to the mesh of the next tooth. In one circle, the rotation angle of the pinon is 7.826°. The angle is divided into 10 parts equally, and 11

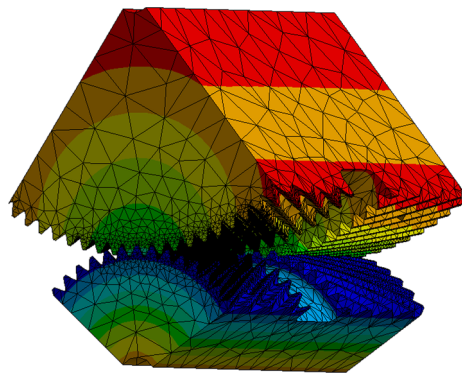

**Fig. 4** Finite element model of the herringbone gear pair

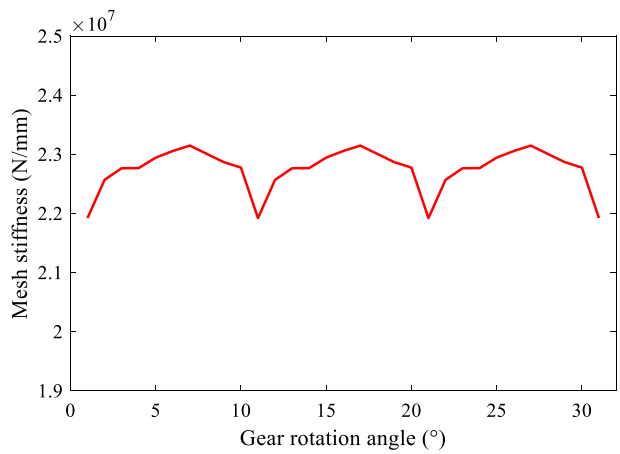


**Fig. 5** Mesh stiffness of the herringbone pair

discrete angle positions are obtained. Each angle position is loaded and solved, and the angular deformation is extracted. Then, the torsional mesh stiffness $K_T$ can be calculated

$$K_{\mathrm{T}} = \frac{T_{\mathrm{m}}}{\Delta\theta}. \tag{17}$$

where $T_{\mathrm{m}}$ is the drag torque; $\Delta\theta$ is the angular deformation of gear mesh point.

The $F_n$ and $\Delta\theta$ can be calculated by the following equations

$$F_{\mathrm{n}} = \frac{T_{\mathrm{m}}}{r_{\mathrm{p}} \cos\alpha_{\mathrm{n}} \cos\beta_{\mathrm{pg}}}, \quad \Delta_\theta = \frac{\delta_{\mathrm{n}}}{r_{\mathrm{p}}}, \tag{18}$$

where $r$ is the indexing circle radius of the pinon; $\alpha_n$ is the normal pressure angle.

Substituting Eqs. (16) and (18) to Eq. (17), the mesh stiffness can be obtained

$$K_n = K_T . \frac{4\cos\beta_{\mathrm{pg}}}{\left(m_n z_{\mathrm{p}}\right)^2 \cos\alpha_n}, \tag{19}$$

where $m_{\mathrm{n}}$ the normal modulus; $z_{\mathrm{p}}$ is the teeth number of the pinion.

With a drag torque of 26191 Nm, the equivalent meshing stiffness of three complete mesh cycles is obtained according to the above method, as shown in Fig. 5. For the convenience of modeling, the average mesh stiffness is $K_{\mathrm{m}} = 2.28 \times 10^7$ N/mm. By substituting this stiffness value to Eq. (10), the gear meshing stiffness matrix can be obtained.

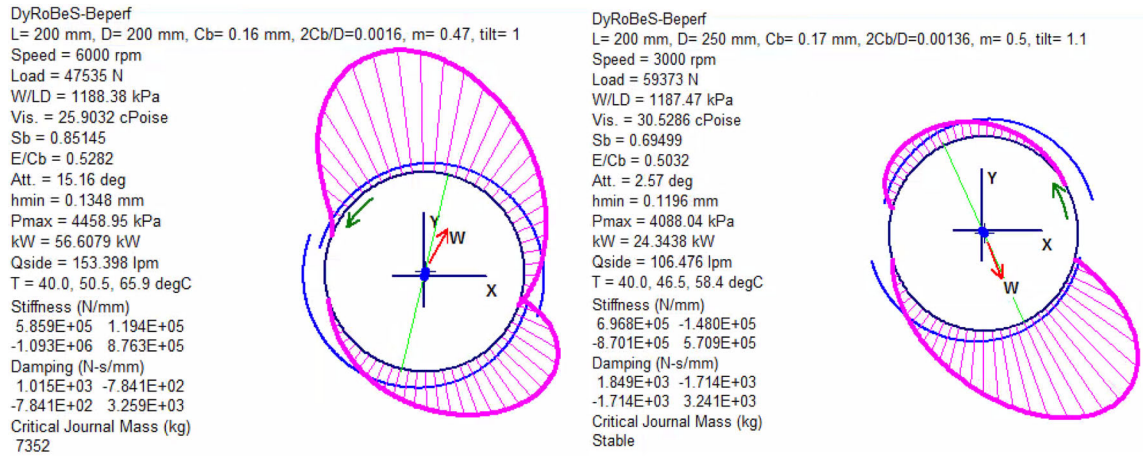


(a) Bearing 1 and 2 (b) Bearing 3 and 4

**Fig. 6** Calculation results of the bearing stiffness and damping

**Table 2** Bearing stiffness and damping

| | Bearing 1 and 2 | Bearing 3 and 4 |
|---|---|---|
| Stiffness (N/mm) | $k_{xx} = 5.859 \times 10^5$ $k_{xy} = 1.194 \times 10^5$ | $k_{xx} = 6.968 \times 10^5$ $k_{xy} = -1.480 \times 10^5$ |
| | $k_{yx} = -1.093 \times 10^5$ $k_{yy} = 8.763 \times 10^5$ | $k_{yx} = -8.701 \times 10^5$ $k_{yy} = 5.709 \times 10^5$ |
| Damping (N-s/mm) | $c_{xx} = 1.015 \times 10^3$ $c_{xy} = -7.841 \times 10^5$ | $c_{xx} = 1.849 \times 10^3$ $c_{xy} = -1.714 \times 10^5$ |
| | $c_{yx} = -7.841 \times 10^2$ $c_{yy} = 3.259 \times 10^3$ | $c_{yx} = -1.714 \times 10^2$ $c_{yy} = 3.241 \times 10^3$ |

## 2.3 Bearing model

In this subsection, the DyRoBeS software is applied to calculate the stiffness and damping of the bearing. DyRoBeS is a commercial software for bearing and rotor dynamic characteristics analysis, which is widely used in rotor dynamic field.

The fluid film journal bearings are used in the investigated herringbone gear transmission system. For simplicity, the bearing is simplified to massless spring and damping. The stiffness and damping of the bearings can be obtained by using the DyRoBeS bearing module. The calculation results are shown in Fig. 6 and Table 2. According to the node position of the bearing in the actual transmission system, the stiffness and damping matrix of the bearings are then integrated to the system matrix.

## 2.4 Gear-shaft-bearing model

The mass matrix, damping matrix, gyroscopic matrix, stiffness matrix and mesh effect of each shaft segment, as well as the stiffness and damping matrix of bearings are assembled according to the node position, and the dynamic equation of the system is obtained.

$$\boldsymbol{M}\ddot{\boldsymbol{X}} + (\boldsymbol{C} + \Omega \boldsymbol{G})\dot{\boldsymbol{X}} + \boldsymbol{K}\boldsymbol{X} = \boldsymbol{q}, \tag{20}$$

where $\boldsymbol{M}, \boldsymbol{C}, \boldsymbol{G}$, and K are the mass matrix, damping matrix, gyroscopic matrix and stiffness matrix of the system, respectively; $\boldsymbol{q}$ is the excitation includes static transmission error excitation and external torque excitation.

Equation (20) can be transformed into frequency domain analysis and expressed as

$$\boldsymbol{A}(\omega)\boldsymbol{X}(\omega) = \boldsymbol{Q}(\omega), \tag{21}$$

where

$$\boldsymbol{A}(\omega) = -\omega^2 \boldsymbol{M} + i\omega(\boldsymbol{C} + \boldsymbol{G}) + \boldsymbol{K}, \tag{22}$$

$$\boldsymbol{X} = Xe^{i\omega t}, \boldsymbol{Q} = Qe^{i\omega t}, \tag{23}$$

## 3 Uncertainty model

The model parameters such as mass, stiffness and damping in Eq. (20) are uncertain due to the influence of geometric factors or material parameters. These factors lead to the uncertainty of the response of the system. Therefore, in the dynamic analysis of gear-rotor system, the $\boldsymbol{A}$, $\boldsymbol{X}$, and $\boldsymbol{Q}$ should be regarded as a random process. If the uncertain parameters in the gear rotor system are represented as random variables, the stochastic dynamics equation of the system can be expressed as

$$\boldsymbol{A}(\tau)\boldsymbol{X}(\tau) = \boldsymbol{Q}(\tau), \tag{24}$$

where

$$\boldsymbol{A}(\tau) = -\omega^2\boldsymbol{M}(\tau) + i\omega(\boldsymbol{C}(\tau) + \boldsymbol{G}(\tau)) + \boldsymbol{K}(\tau), \tag{25}$$

where $\tau$ is the random characteristic of the uncertain parameters.

There are many methods for uncertainty analysis of stochastic processes, the most common of which is Monte Carlo method. However, the MCS method has a large amount of calculation, thus it is usually used as a reference method for uncertainty analysis. PCE method is a relative novel method for uncertainty analysis. With its good mathematical basis and the ability to accurately describe the randomness of random variables with arbitrary distribution, PCE has been more and more widely used in the field of dynamic analysis in recent years [29]. PCE is an uncertainty propagation method based on polynomial chaotic theory. It possesses good mathematical basis and the ability to accurately describe the randomness of random variables with arbitrary distribution. In PCE, the sum of orthogonal polynomials corresponding to the distribution of input parameters is used to approximately represent a random output process. In this section, the PCE method is used to construct the uncertainty model of the gear system.

### 3.1 Model building

The Askey scheme is the foundation of PCE model construction [30]. It points out the optimal orthogonal polynomial basis function corresponding to different distribution types of random variables. The PCE model can be constructed by selecting the corresponding orthogonal basis function according to the distribution type of input variables. For a random variable $Y$, the Hermite polynomial can be expressed as

$$\begin{aligned} Y(\theta) = c_0 I_0 &+ \sum_{i_1=1}^{\infty} c_{i_1} I_1\big(\xi_{i_1}(\theta)\big) + \sum_{i_1=1}^{\infty}\sum_{i_2=1}^{i_1} c_{i_1 i_2} I_2\big(\xi_{i_1}(\theta), \xi_{i_2}(\theta)\big), \\ &+ \sum_{i_1=1}^{\infty}\sum_{i_2=1}^{i_1}\sum_{i_3=1}^{i_2} c_{i_1 i_2 i_3} I_3\big(\xi_{i_1}(\theta), \xi_{i_2}(\theta), \xi_{i_3}(\theta)\big) + \cdots \end{aligned} \tag{26}$$

where $\theta$ represents the random variable, which will be omitted in the following equations for simplicity; $I_n\big(\xi_{i_1}(\theta), \xi_{i_2}(\theta), \ldots, \xi_{i_n}(\theta)\big)$ denotes a mixed orthogonal polynomial of order $n$, which is a function of multi-dimensional standard random variables $\xi_{i_1}, \xi_{i_2}, \ldots, \xi_{i_n}$.

In general, the dimension of $\xi = [\xi_{i_1}, \xi_{i_2}, \ldots, \xi_{i_n}]$ is the same as that of the random input variable $X = [X_1, X_2, \ldots, X_n]$ in the original random space. Therefore, Eq. (26) can be simplified as

$$Y = \sum_{i=0}^{\infty} c_i \psi_i(\xi). \tag{27}$$

where $C_i$ and $\psi_i$ correspond to $\alpha_{i_1 i_2 \ldots i_n}$ and $I_n\big(\xi_{i_1}, \xi_{i_2}, \xi_{i_3}, \ldots\big)$ in Eq. (27), respectively; $C_i$ is the chaotic polynomial coefficient to be solved, when it is calculated, MCS can be run on the chaotic polynomial model, and the random probability characteristic of the output response $Y$ can be obtained.

The number of terms in Eq. (27) is infinite, in order to reduce the amount of calculation, it is usually truncated at a certain order $p$, and the corresponding model can be expressed as

$$\widehat{Y} = \sum_{i=0}^{P} c_i \psi_i(\xi). \tag{28}$$

The number of coefficients in a truncated polynomial can be determined by the following equation

$$N = \frac{(d+p)!}{d!\,p!}. \tag{29}$$

where $d$ is the dimension of the random variable.

The random parameters can be expanded by Karhunen–Loeve method, and the stochastic dynamic equation of gear-rotor system is obtained

$$\left(\sum_{i=0}^{\infty}\{A\}_i\psi_i(\xi(\tau))\right)\left(\sum_{j=0}^{\infty}\{X\}_j\psi_j(\xi(\tau))\right) = \left(\sum_{k=0}^{\infty}\{Q\}_k\psi_k(\xi(\tau))\right), \tag{30}$$

where $\psi_i(\xi(\tau))$ denotes the chaotic orthogonal polynomial of order $p$, which is composed of the product of 1-dimensional orthogonal polynomial corresponding to each dimensional random variable; $\{A\}_{nn}$ represents the coefficient of the $nn$'th orthogonal polynomial corresponding to $\psi_{nn}(\xi(\tau))$ and $nn = i,j,k$.

### 3.2 PCE coefficients calculation

In this subsection, the stochastic response surface method (SRSM) is used to calculate the PCE coefficients. The calculation process is mainly divided into three steps: the selection of sample points, the calculation of response value and the estimation of PCE coefficient.

The Latin hypercube design (LHD) approach is used to extract the sample points. The sampling points should be selected in the standard random space, which means that each dimension in the space is a standard random variable from the Askey scheme. Selecting $N$ sample points in the standard random space can be expressed as

$$\boldsymbol{\xi}^s = \left[\xi_1^s, \cdots, \xi_j^s, \cdots, \xi_N^s\right]^T. \tag{31}$$

The original random variable is usually not a standard random variable. In order to obtain the real response value, the sampling point on the standard random space $\boldsymbol{\xi}$ should be transformed into its original random space $X$

$$\mathrm{X}^s = \left[X_1^s, \cdots, X_j^s, \cdots, X_N^s\right]^{\mathrm{T}}. \tag{32}$$

The transformed sample points are then brought into the original response function, and the response value at the sample is

$$F(X) = \left[F\left(X_1^s\right), \cdots, F\left(X_j^s\right), \cdots, F\left(X_N^s\right)\right]^T. \tag{33}$$

The PCE coefficients can be estimated by least quadratic regression method. The sample points and function response values are substituted into (28), and the following equation can be obtained

$$\boldsymbol{Ac} = \boldsymbol{Y}. \tag{34}$$

where

$$\boldsymbol{A} = \begin{bmatrix} \Phi_0\left(\xi_1^s\right) & \Phi_1\left(\xi_1^s\right) & \cdots & \Phi_P\left(\xi_1^s\right) \\ \Phi_0\left(\xi_2^s\right) & \Phi_1\left(\xi_2^s\right) & \cdots & \Phi_P\left(\xi_2^s\right) \\ \vdots & \vdots & \cdots & \vdots \\ \Phi_0\left(\xi_N^s\right) & \Phi_1\left(\xi_N^s\right) & \cdots & \Phi_P\left(\xi_3^s\right) \end{bmatrix}. \tag{35}$$

$$\boldsymbol{c} = \begin{bmatrix} c_0 \\ c_1 \\ \vdots \\ c_N \end{bmatrix}. \tag{36}$$

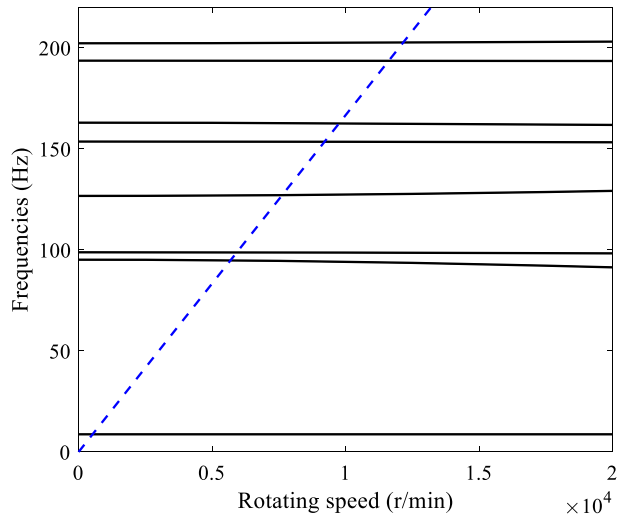


**Fig. 7** Campbell diagram of the system

$$\boldsymbol{Y} = \begin{bmatrix} F\left(X_1^s\right) \\ F\left(X_2^s\right) \\ \vdots \\ F\left(X_N^s\right) \end{bmatrix}. \tag{37}$$

According to the least square regression, the PCE coefficient can be calculated

$$\boldsymbol{c} = \left(AA^T\right)^{-1} A^T \boldsymbol{Y}. \tag{38}$$

## 4 Uncertainty analysis of vibration response

The mesh stiffness and bearing stiffness are important parameters that affect the dynamic characteristics of gear rotor system. In engineering, due to assembly error, bearing clearance tolerance, gear wear, operating conditions and other factors, the mesh stiffness and bearing stiffness and damping of gear system are actually uncertain parameters, which will lead to errors if deterministic parameters are used in dynamic modeling. In this section, the uncertainty of gear rotor vibration response is investigated by considering the uncertainty of meshing stiffness, bearing stiffness and damping.

The dynamic model of the herringbone gear rotor system with deterministic parameters in Table 1 is established and solved. The Campbell diagram of the system is then obtained and shown in Fig. 7. The first eight critical speeds of the system are 525 r/min, 5709 r/min, 5929 r/min, 7603 r/min, 9217 r/min, 116,190 r/min, 12135 r/min, respectively. It can be seen that the gear rotor system will experience many oscillations when increasing speed. The frequency response of each node of the system is shown in Fig. 8. In order to facilitate the analysis, the vibration response in the X direction of node 11 is selected to study. At the same time, the third critical speed 5929r/min and its nearby speed region [5600 6100] r/min are selected to study, and the corresponding vibration response is shown in Fig. 9. It should be pointed out that logarithmic coordinates are used here to better reflect the variation of amplitude with rotational speed.

### 4.1 Mesh stiffness uncertainty

Considering the uncertainty of the meshing stiffness, it is expressed as interval parameters [$k_{\mathrm{m}}$-$\xi_{\mathrm{km}}$ $k_{\mathrm{m}}$, $k_{\mathrm{m}}$ + $\xi_{\mathrm{km}}$ $k_{\mathrm{m}}$], $k_{\mathrm{m}}$ and $\xi_{\mathrm{km}}$ are average meshing stiffness and deviation coefficient, respectively. The order $p$ of PCE is set to 6 in this paper and the results are compared with those obtained with the Monte Carlo method (20,000 samplings). It can be seen from Fig. 10, when $\xi_{\mathrm{km}} = 0.1$, the PCE-mean curves are superposed almost perfectly with those of Monte Carlo. It should be noted that only $\xi_{\mathrm{km}} = 0.1$ is selected here for simplicity.

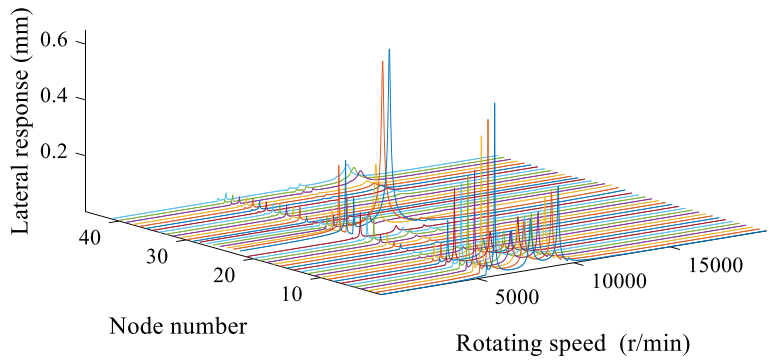


**Fig. 8** Frequency response of the system

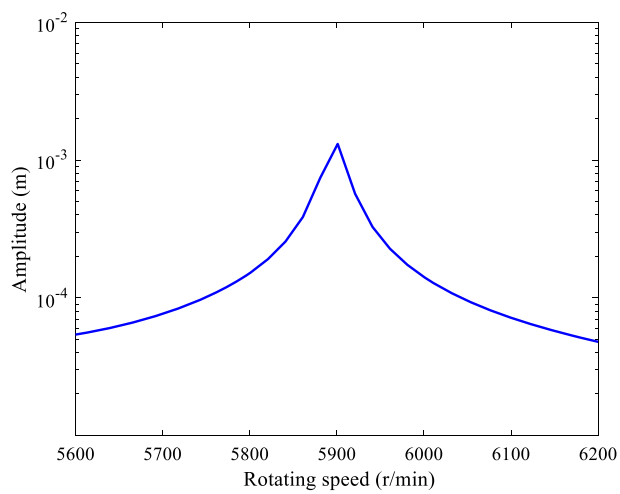


**Fig. 9** Vibration amplitude of the system with deterministic parameters

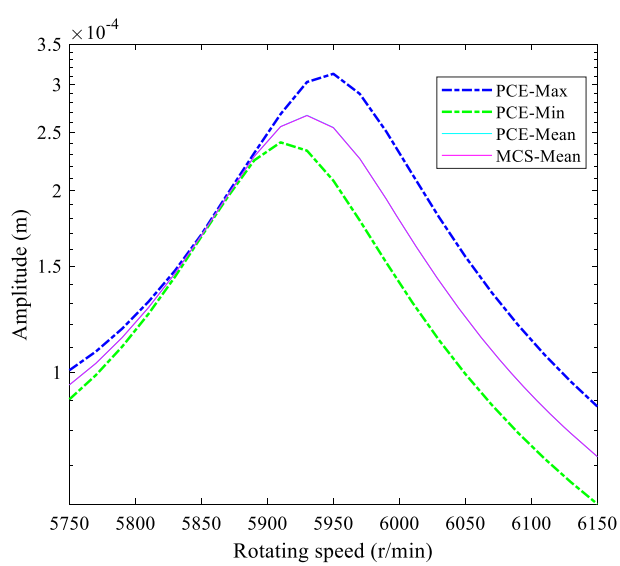


**Fig. 10** Amplitude–frequency response of the system with uncertain mesh stiffness when $\xi_{\mathrm{km}} = 0.1$

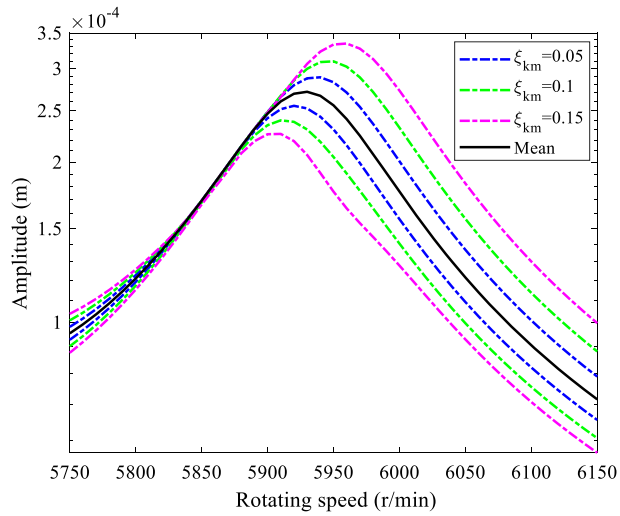


**Fig. 11** Amplitude–frequency response of the system with uncertain mesh stiffness

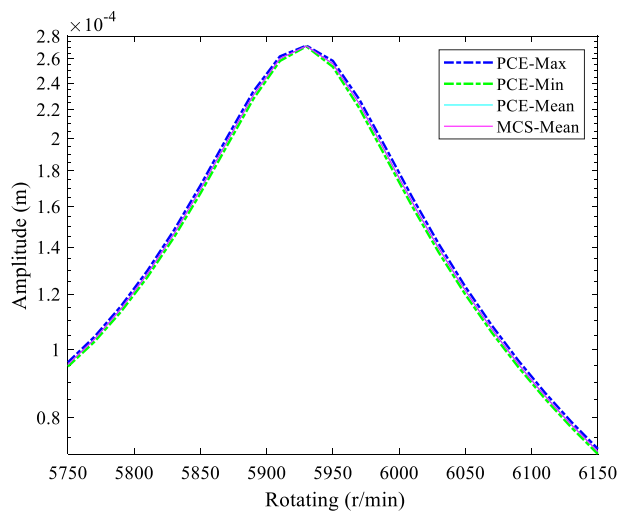


**Fig. 12** Amplitude–frequency response of the system with uncertain bearing stiffness when $\xi_{\mathrm{kb}} = 0.1$

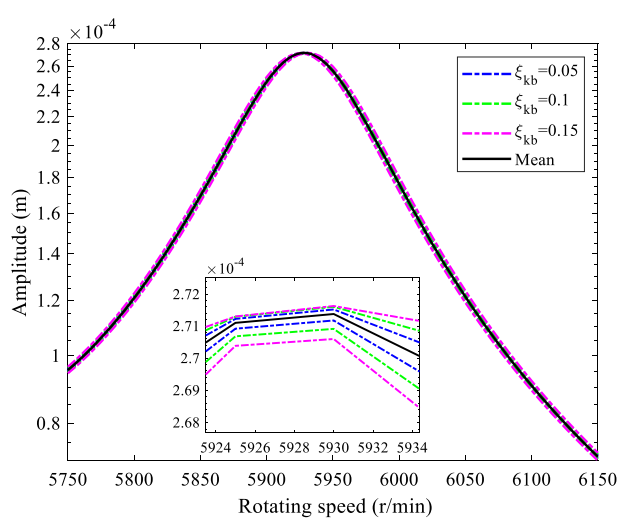


**Fig. 13** Amplitude–frequency response of the system with uncertain bearing stiffness

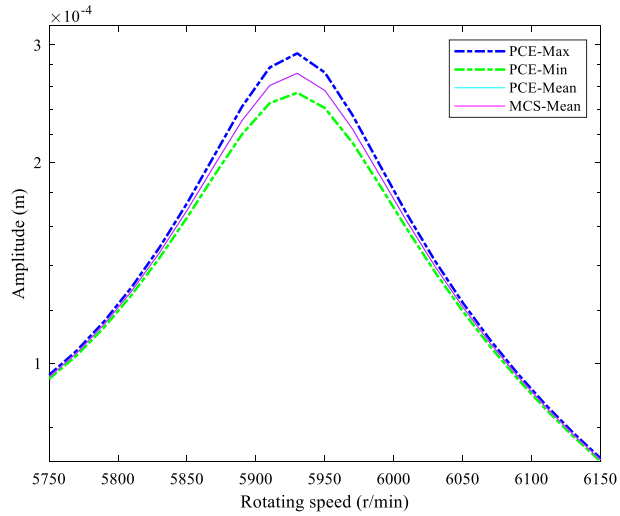


**Fig. 14** Amplitude–frequency response of the system with uncertain bearing damping when $\xi_{cb} = 0.1$

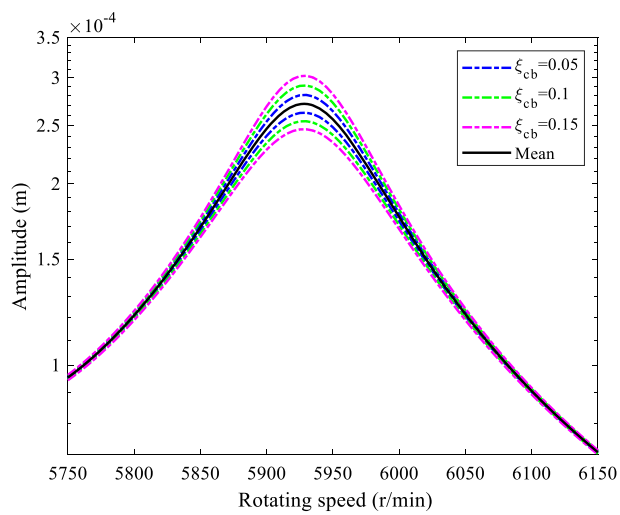


**Fig. 15** Amplitude–frequency response of the system with uncertain bearing damping

When $\xi_{km} = 0.05$, 0.1 and 0.15, the upper and lower boundaries of the amplitude–frequency response of the system are obtained as shown in Fig. 11. Note that the sampling points are encrypted here for better comparison. It can be seen that the interval value of the vibration amplitude increases with the increase of $\xi_{km}$, especially near the resonance region of the system, which indicates that the dynamic characteristics of the system near the resonance region are more sensitive to the uncertainty of mesh stiffness. It can also be found that when $\xi_{km}$ increases, the upper boundary of the response region of the resonance region shifts to the right and the lower boundary of the region shifts to the left, compared with the system response results under deterministic parameters. This is mainly because the mesh stiffness leads to the change of the natural frequency, which has a direct impact on the resonance peak.

## 4.2 Bearing stiffness uncertainty

Considering the uncertainty of the bearing stiffness, in order to simplify the analysis, the four stiffnesses of the bearing take the same deviation coefficient. The uncertainty of bearing stiffness can be expressed as [$k_b$-$\xi_{kb}k_b$, $k_b + \xi_{kb}k_b$], $k_b$ and $\xi_{kb}$ are the average bearing stiffness and deviation coefficient, respectively. It can be seen from Fig. 12, when $\xi_{kb} = 0.1$, the PCE-mean curves are superposed almost perfectly with those of Monte Carlo method. When $\xi_{kb} = 0.05$, 0.1 and 0.15, the upper and lower boundaries of the amplitude–frequency response

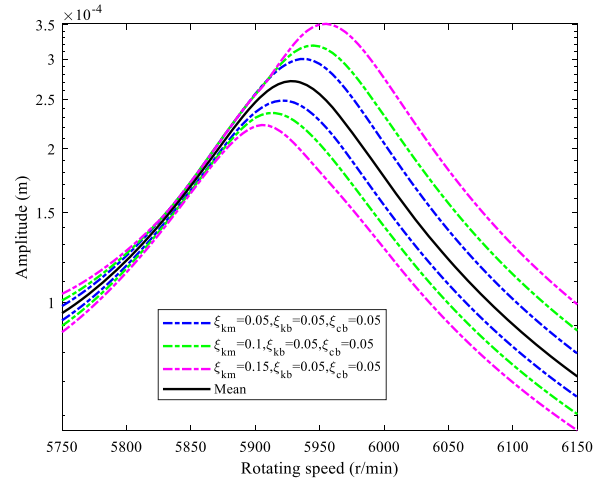


(a)

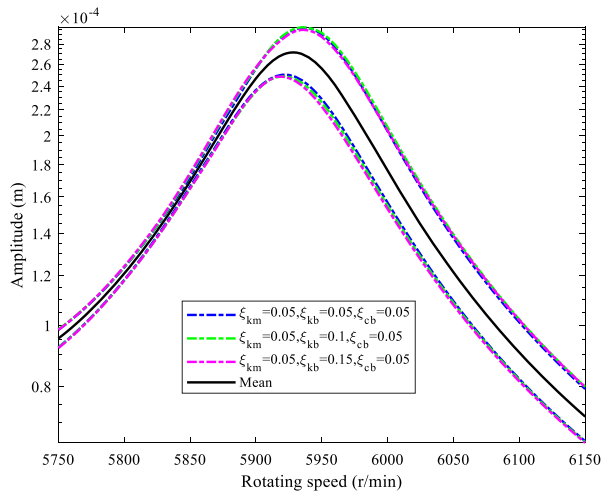


(b)

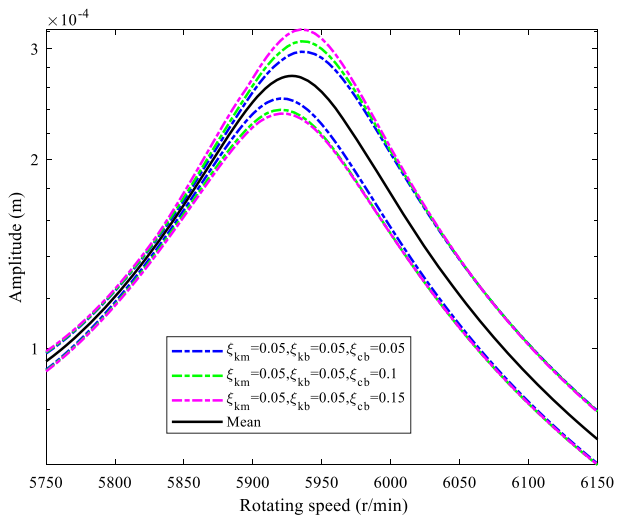


(c)

**Fig. 16** Amplitude–frequency response of the system with hybrid uncertainty. **a** Amplitude–frequency response with $\xi_{km} = 0.05$, 0.1, 0.15 and $\xi_{kb} = \xi_{cb} = 0.05$. **b** Amplitude–frequency response with $\xi_{kb} = 0.05$, 0.1, 0.15 and $\xi_{km} = \xi_{cb} = 0.05$. **c** Amplitude–frequency response with $\xi_{cb} = 0.05$, 0.1, 0.15 and $\xi_{km} = \xi_{kb} = 0.05$

of the system are obtained as shown in Fig. 13. It can be seen that there is no obvious deviation between the upper and lower boundary values of the vibration amplitude of the system, indicating that the uncertainty of bearing stiffness has little influence on the frequency domain response of the gear system.

### 4.3 Bearing damping uncertainty

Considering the uncertainty of the bearing damping, the four dampings take the same deviation coefficient. The uncertainty of bearing damping can be expressed as $[c_b\text{-}\xi_{cb}\ c_b,\ c_b + \xi_{cb}\ c_b]$, $c_b$ and $\xi_{cb}$ are the average damping and deviation coefficient of bearing, respectively. It can be seen from Fig. 14, when $\xi_{cb} = 0.1$, the PCE-mean curves are superposed almost perfectly with those of Monte Carlo. When $\xi_{cb} = 0.05$, 0.1 and 0.15, the vibration response of the system is obtained as shown in Fig. 15. It can be seen that there is no obvious deviation between the upper and lower boundary values of the vibration amplitude of the system. In addition, the impact of the uncertainty of bearing damping on the frequency domain response of the system is mainly concentrated in the resonance region, but has no obvious effect on other speed regions. The reason for this difference is that changing the bearing damping will change the amplitude of the dynamic response, especially in the resonance region.

### 4.4 Hybrid uncertainty

Considering the uncertainty of gear meshing stiffness, bearing stiffness and damping, taking different deviation coefficients, the amplitude–frequency response of the system is obtained as shown in Fig. 16. It can be seen that the upper and lower boundary values of the vibration amplitude of the system are obviously offset under different deviation coefficients. In Fig. 16a, the deviation of the upper and lower boundary value of the system amplitude is the most obvious when $\xi_{km}$ changes, indicating that the uncertainty of mesh stiffness has a greater influence on the natural frequency of the system. The deviations of the upper and lower limits of the system amplitude in Fig. 16b and c are mainly due to the impact of $\xi_{km}$. In addition, the amplitude variation in Fig. 16c is more obvious than that in Fig. 16b. This is mainly because the uncertainty of bearing damping has a greater influence on the amplitude of the dynamic response of the system.

## 5 Conclusions

There are a large number of uncertainties in the gear transmission system, which makes the stiffness, damping and load parameters of the system have a certain degree of uncertainty. It is of great significance for gear system design and reliability analysis to correctly estimate the influence of these uncertain parameters on the dynamic characteristics of the system. In this paper, the dynamic models of gear, shaft and bearing aiming in a herringbone gear transmission system, are established, respectively, and the dynamic model of the system is obtained after integration. The uncertainty of the system is modeled by the PCE method, and the influence of the uncertain parameters on the vibration response of the system is analyzed. The main conclusions are as follows:

1. The influence level of the uncertainty of different parameters is different. With the increase of the uncertainty of mesh stiffness, the upper boundary of the vibration response region of the system resonance region shifts to the right and the lower boundary of the interval shifts to the left.
2. The influence of the uncertainty of bearing damping on the frequency domain response of the system is mainly concentrated in the resonance region, but has no obvious effect on other speed regions. The uncertainty of bearing stiffness has little influence on the system response.
3. The influence of mixed uncertainty on the vibration response of the system is comprehensive, and the greater the uncertainty deviation coefficient of a parameter, the greater the influence on the vibration response of the system.

**Acknowledgements** This work was supported by the National Key Research and Development Program of China (2020YFB2008101) and the National Natural Science Foundation of China (12072106 and 52005156).

**Declarations**

**Conflict of interest** The authors declare no conflict of interest.

## References


1. Liu, C.Z., Qin, D.T., Liao, Y.H.: Dynamic model of variable speed process for herringbone gears including friction calculated by variable friction coefficient. J. Mech. Des. **136**(4), 041006 (2014)
2. Liang, X.H., Zuo, M.J., Feng, Z.P.: Dynamic modeling of gearbox faults: a review. Mech. Syst. Signal Process. **98**, 852–876 (2018)
3. Bruzzone, F., Rosso, C.: Sources of Excitation and models for cylindrical gear dynamics: a review. Machines **8**, 37 (2020)
4. Choi, S.H., Glienicke, J., Han, D.C., et al.: Dynamic gear loads due to coupled lateral, torsional and axial vibrations in a helical gearedsystem. J. Vib. Acoust. **121**(2), 141–148 (1999)
5. Sondkar, P., Kahraman, A.: A dynamic model of a double-helical planetary gear set. Mech. Mach. Theory **70**, 157–174 (2013)
6. Chen, S.Y., Tang, J.Y., Li, Y.P., et al.: Rotordynamics analysis of a double-helical gear transmission system. Meccanica **51**(1), 251–268 (2016)
7. Chen, S.Y., Tang, J.Y.: Effects of staggering and pitch error on the dynamic response of a double-helical gear set. J. Vib. Control **23**(11), 1844–1856 (2017)
8. Wang, C., Fang, A.D., Jia, H.T.: Investigation of a design modification for double helical gears reducing vibration and noise. J. Mar. Sci. Appl. **9**(1), 81–86 (2010)
9. Dong, J.C., Wang, S.M., Lin, H., et al.: Dynamic modeling of double-helical gear with Timoshenko beam theory and experiment verification. Adv. Mech. Eng. **8**(5), 1–14 (2016)
10. Wang, C., Wang, S.R., Yang, B., et al.: Dynamic modeling of double helical gears. J. Vib. Control **24**(17), 3989–3999 (2018)
11. Liu, C., Fang, Z.D., Wang, F., et al.: An improved model for dynamic analysis of a double-helical gear reduction unit by hybrid user-defined elements: experimental and numerical validation. Mech. Mach. Theory **127**, 96–111 (2018)
12. Yin, M.H., Chen, G.D., Su, H.: Theoretical and experimental studies on dynamics of double-helical gear system supported by journal bearings. Adv. Mech. Eng. **8**(5), 1–13 (2016)
13. Yin, M.H., Cui, Y.H., Meng, X.J., et al.: Dynamic analysis of double-helical gear system considering effect of oil film among meshing teeth. Adv. Mech. Eng. **12**(5), 1–14 (2020)
14. Schuëller, G.I., Pradlwarter, H.J.: Uncertain linear systems in dynamics: retrospective and recent developments by stochastic approaches. Eng. Struct. **31**(11), 2507–2517 (2009)
15. Simoen, E., Roeck, G.D., Lombaert, G.: Dealing with uncertainty in model updating for damage assessment: a review. Mech. Syst. Signal Process. **56–57**(56), 123–149 (2015)
16. Chao, F., Jjs, B., Wz, C., et al.: A state-of-the-art review on uncertainty analysis of rotor systems. Mech. Syst. Signal Process. **183**, 109619 (2023)
17. Wei, S., Zhao, J.S., Han, Q.K., Chu, F.L.: Dynamic response analysis on torsional vibrations of wind turbine geared transmission system with uncertainty. Renew. Energy **78**, 60–67 (2015)
18. Guerine, A., Hami, A., Walha, L., et al.: A polynomial chaos method for the analysis of the dynamic behavior of uncertain gear friction system. Eur. J. Mech. **59**, 76–84 (2016)
19. Yang, J.: Vibration analysis on multi-mesh gear-trains under combined deterministic and random excitations. Mech. Mach. Theory **59**, 20–33 (2013)
20. Beyaoui, M., Tounsi, M., Abboudi, K., et al.: Dynamic behaviour of a wind turbine gear system with uncertainties. Comptes Rendus Mécanique **344**(6), 375–387 (2016)
21. Bel, M.I., El Hami, A., Walha, L., et al.: Dynamic response analysis of Vertical Axis Wind Turbine geared transmission system with uncertainty. Eng. Struct. **139**, 170–179 (2017)
22. Fang, Y., Liang, X., Zuo, M.: Effects of friction and stochastic load on transient characteristics of a spur gear pair. Nonlinear Dyn. **93**(2), 599–609 (2018)
23. Hajnayeb, A., Sun, Q.: Study of gear pair vibration caused by random manufacturing errors. Arch. Appl. Mech. **92**, 1451–1463 (2022)
24. Wei, S., Chu, F., Ding, H., et al.: Dynamic analysis of uncertain spur gear systems. Mech. Syst. Signal Process. **150**, 107280 (2021)
25. Fu, C., Lu, K., Xu, Y., et al.: Dynamic analysis of geared transmission system for wind turbines with mixed aleatory and epistemic uncertainties. Appl. Math. Mech. **43**(2), 275–294 (2022)
26. Han, Q., Zhao, J., Chu, F., et al.: Dynamic analysis of a geared rotor system considering a slant crack on the shaft. J. Sound Vib. **331**, 5803–5823 (2012)
27. Marafona, J.D., et al.: Mesh stiffness models for cylindrical gears: a detailed review. Mech. Mach. Theory **166**, 104472 (2021)
28. Yang, Y., Wei, J., Lai, Y., et al.: Vibration response analysis of helical gear transmission considering the tip relief. J. Chongqing Univ. **40**(1), 30–40 (2017)
29. ElHami, A., Guerine, A., Walha, L., et al.: A polynomial chaos method for the analysis of the dynamic behavior of uncertain gear friction system. Eur. J. Mech. A. Solids **59**(4), 76–84 (2016)
30. Xiu, D., Karniadakis, G.: The Wiener-Askey polynomial chaos for stochastic differential equations. SIAM J. Sci. Comput. **24**, 619–644 (2002)

**Publisher's Note** Springer Nature remains neutral with regard to jurisdictional claims in published maps and institutional affiliations.

Springer Nature or its licensor (e.g. a society or other partner) holds exclusive rights to this article under a publishing agreement with the author(s) or other rightsholder(s); author self-archiving of the accepted manuscript version of this article is solely governed by the terms of such publishing agreement and applicable law.